Available online at www.sciencedirect.com
SCIENCE DIRECT®
Journal of Nuclear Materials 322 (2003) 66–72
journal of nuclear materials
www.elsevier.com/locate/jnucmat

Dissolution and precipitation behavior of hydrides in Zircaloy-2 and high Fe Zircaloy

K. Une *, S. Ishimoto

Global Nuclear Fuel-Japan Co. Ltd., 2163 Narita-cho, Oarai-machi, Higashi Ibaraki-gun, Ibaraki-ken 311-1313, Japan

Received 15 July 2002; accepted 29 June 2003

Abstract

In order to elucidate the terminal solid solubility during the dissolution of hydrides at heatup (TSSD) and during the precipitation of hydrides at cooldown (TSSP) for hydrogenated Zircaloy-2 and high Fe Zircaloy, differential scanning calorimetry (DSC) measurements have been carried out in the temperature range of 50–600 °C. The hydrogen concentrations in the two kinds of alloys ranged from 40 to 542 ppm. There was no difference in either TSSD or TSSP solvi between Zircaloy-2 and high Fe Zircaloy, and best-fit equations were derived for the two curves. In the present TSSP data, two different activation energies, separating into high and low temperature ranges at 260 °C, were obtained. Based on the widths of the DSC peak obtained during cooldown, the average precipitation (nucleation plus growth) rates of zirconium hydrides from super-saturated state were assessed. The activation energy of the precipitation rate was approximately equivalent to reported values of hydrogen diffusion coefficients of Zr and Zircaloys.

PACS: 28.41.Bm; 64.75.+g

1. Introduction

Zr alloy claddings used in light water reactors pick up hydrogen during operation; this hydrogen is liberated from the corrosion reaction with water. When the hydrogen concentration in the claddings at any point exceeds the terminal solid solubility (TSS), zirconium hydride is precipitated, which brings about a marked ductility reduction of the claddings. In particular, radially-oriented hydrides drastically reduce the circumferential ductility. Occurrence of unfavorable cracking in Zr alloys has been observed in reactor operation, e.g., delayed hydride cracking in Zr–2.5%Nb pressure tubes of the CANDU reactor [1,2], secondary degraded cracking in BWR claddings after primary fuel failure [3,4] and outside-in type cracking in high burnup BWR claddings arising at power ramp tests [5,6]. Therefore, many studies on hydrogen behavior for Zr alloys have been carried out in the past 40 years.

The solvus for dissolution of hydrides (TSSD) during heating and the solvus for precipitation of hydrides (TSSP) during cooling have been the subjects of many reports [7–15] for Zr and its alloys, and various measuring techniques have been used. However, there is considerable scatter in the published TSS data. This may be attributed partly to the different experimental techniques used such as dilatometry, calorimetry, and measurements of diffusion gradient/equilibrium, dynamic elastic modulus, internal friction, and so on. Another factor for this may arise from the difference in temperature history applied to samples. Moreover, most of these data are devoted to TSSD, fewer TSSP data have been reported. Consequently, systematic data sets of TSSD and TSSP solvi using the same technique and sample are needed for the appropriate evaluation of dissolution/precipitation behavior of hydrides during heatup and cooldown stages, because the large hysteresis

* Corresponding author. Tel.: +81-29 267 9011; fax: +81-29 267 9014.
E-mail address: katsumi.une@gnf.com (K. Une).

0022-3115/$ - see front matter © 2003 Elsevier B.V. All rights reserved.
doi:10.1016/S0022-3115(03)00320-9

existing between TSSD and TSSP plays an important role in the above hydride-assisted cracking of Zr alloys. Beside these solubility data, kinetic data such as precipitation and dissolution rates, and diffusion rate, are needed to model overall hydrogen behavior in Zr alloys.

New Zr alloys for use as BWR fuel claddings and spacer materials at high burnups, have been developed from the viewpoint of improvement of corrosion resistance and hydrogen pickup properties. One promising candidate is high Fe Zircaloy, which has an increased amount of Fe above the upper limit of the Zircaloy-2 chemical specification. In our previous irradiation tests in commercial BWRs and test reactors, it gave better performances than Zircaloy-2 [16]. Therefore, systematic TSS and kinetic data for this new alloy as well as the currently produced Zircaloy-2 are needed.

In the present study, a data set of TSSD and TSSP for the current Zircaloy-2 and improved high Fe Zircaloy for BWRs, which were hydrogenated up to a level of 542 ppm, were derived by differential scanning calorimetry (DSC), and best fit equations for the two solvi were presented. Moreover, the average precipitation rates of zirconium hydrides from the super-saturated state were assessed from the widths of the DSC peak obtained during cooldown.

2. Experimental

2.1. Materials

Table 1 shows the chemical composition of Zircaloy-2 and high Fe Zircaloy plates, which were used for the present TSS measurements. The two plates were fabricated by cold rolling and a heat treatment process, in the same way as the current Zircaloy-2 cladding. The final annealing temperature was 575 °C, bringing about a recrystallized grain structure. The hydrogen contents of the as-received materials were 25–30 ppm.

Test samples were hydrided by two methods. One was gaseous hydrogenation at 300 °C in an Ar/3%H_2 mixed gas, and absorbed hydrogen concentrations were controlled by varying reaction duration. After hydrogen charging, the samples were homogenized at 400 °C for 8 h in pure Ar. The other hydrogen charging was carried out by a corrosion reaction in water vapor of 10.3 MPa at 530 °C for reaction durations of one to six days. The former method was applied to prepare lower hydrogen content samples (<100 ppm), and the latter method for higher hydrogen content samples (>100 ppm). After hydriding, the surface corrosion layer was removed by grinding. Then the test samples were cut into shapes approximately 4 mm square and 0.5 mm thick, and weighing about 40–50 mg. The hydrogen concentration in all the samples was chemically analyzed by the hot vacuum extraction method with an accuracy of ±3%, and it ranged from 40 to 542 ppm. For some of the samples, the hydrogen concentration was also analyzed after the DSC measurements. It was confirmed that there was no change in the hydrogen concentration before and after the measurements within the analytical error.

2.2. Differential scanning calorimetry

The TSSD and TSSP temperatures of the samples were measured using the DSC technique. A Netzsch DSC-404 was used for the measurements. The instrument is based on the measurement of thermal response of a sample compared to a reference when the two are heated up or cooled down uniformly at a constant heating or cooling rate. The resulting differential heat flow detects the dissolution or precipitation of hydrides in the samples. Before the DSC measurements, the instrument was calibrated using melting points of four standard metals (In, Bi, Zn and Al). The details of the DSC instrument were described previously [17].

The DSC measurements were carried out in purified Ar at the flow rate of 50 cm^3/min. In all the measurements, a sample was first heated up to 600 °C from 50 °C in Ar, followed by a cooldown to 150 °C, with a hold-time of 5 min at the maximum temperature. In the present study, the heatup/cooldown rate of 10 °C/min was adopted. This rate was chosen because a fast rate provides higher DSC sensitivity, and almost no rate dependence on dissolution/precipitation temperature has been reported in the range of 0.5–10 °C/min [15].

3. Results and discussion

3.1. DSC curves

Fig. 1 shows a typical example of a DSC curve with its time deviation (DDSC) for Zircaloy-2 containing 106 ppm hydrogen, obtained during heatup. In the

Table 1
Chemical compositions of Zircaloy-2 and high Fe Zircaloy

Material	Sn (wt%)	Fe (wt%)	Cr (wt%)	Ni (wt%)	O (wt%)	Zr (wt%)
Zry-2	1.37	0.17	0.11	0.07	0.13	Balance
High Fe Zry	1.46	0.26	0.10	0.05	0.15	Balance

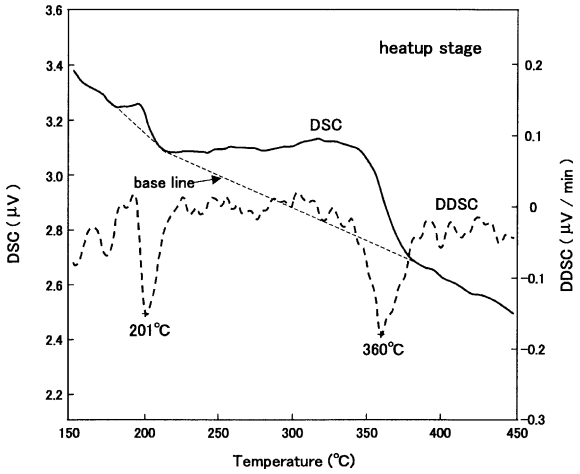

Fig. 1. Typical DSC and time derivation curves from Zircaloy-2 specimen containing 106 ppm hydrogen obtained during heatup (heating rate: 10 °C/min).

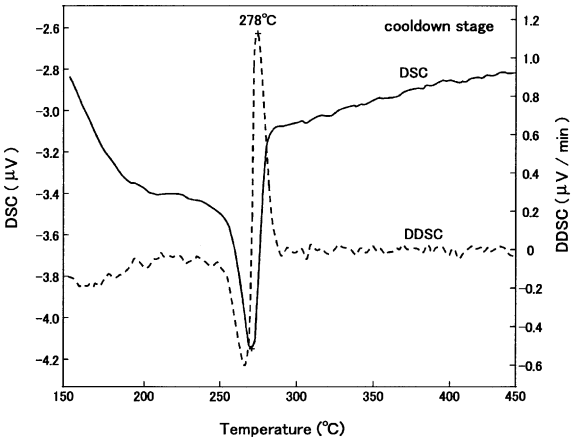

Fig. 2. Typical DSC and time derivation curves from Zircaloy-2 specimen containing 106 ppm hydrogen obtained during cooldown (cooling rate: 10 °C/min).

figure, two endothermic peaks relative to a baseline are detected around 200 °C and in the range of 215–380 °C. The former small peak may result from the phase transformation from γ-ZrH in small amounts to δ-ZrH_x, as discussed later. The latter large and broad peak comes from hydride dissolution. The deviation from the dotted baseline starts around 215, which is related to the heat absorbed during the hydride dissolution. Namely, the heat flow increases with increasing temperature as heat is absorbed by the sample to dissolve hydrides. Once the last hydrides dissolve, the heat absorbed is no longer required and the curve swings downward to the baseline around 380 °C. Some other contributions to DSC heat flow, originating from the evolutions of point defects and dislocations, should be minor based on heat capacity measurements by quantitative DSC mode using the same samples. Namely, enthalpy changes calculated from the second peak areas were consistent with reported thermodynamic dissolution enthalpies, which will be presented in our subsequent paper describing heat capacity of hydrogenated Zircaloys [18].

For this broad peak, three temperatures are noted; namely the peak temperature, the maximum slope temperature (MST) and the completion temperature. There are no established rules and experimental evidence for declaring which temperature best represents the temperature for complete hydride dissolution. Some authors [13,15] chose MST as the TSSD temperature, which corresponds to the maximum of the DDSC curve, due to better correlation between their MST and reported equilibrium TSSD obtained in the diffusion annealing technique [8] and to ease of data analysis. Also in the dynamic elastic modulus measurements, TSS temperature was determined from the derivative of Young's modulus versus temperature [11]. By contrast, the peak temperature of DSC curve was adopted for TSSD in another paper [12]. In the present study, MST was adopted as TSSD temperature based on a good reproducibility originating from the narrower peak in the DDSC curve than the DSC curve and on good agreement with previously reported equilibrium TSSD data [9] (see Fig. 1). Eventually, in the case of Fig. 1, TSSD temperature is 360 °C. However, it must be pointed out that some evaluation errors in TSSD and also TSSP are inherent, depending on choice of the characteristic temperatures.

The corresponding DSC curve obtained on cooldown for the same 106 ppm sample is given in Fig. 2, in which a sharp exothermic peak is seen around 270 °C. The analysis of the DSC curve on cooling is similar to the heating DSC curve, to define the hydride precipitation temperature, and correspondence is made to the MST in the cooldown curve. Therefore, the TSSP temperature is 278 °C. In the case of TSSP, sharp DSC peaks lead to smaller evaluation errors due to choice of the characteristic temperatures. Compared with TSSD temperature of Fig. 1, there is a significant hysteresis between the two temperatures, which is examined in detail later.

3.2. TSSD and TSSP

The Arrhenius plots of the solvi of TSSD and TSSP obtained in the present study are shown in Fig. 3. In addition to the measured TSSD and TSSP solvi, one more assessed solvus for hydride growth denoted as TSSG is added to Fig. 3. The meaning and derivation of TSSG are described in the next section. A statistical analysis of the data in Fig. 3 shows no difference in either TSSD or TSSP solvi between Zircaloy-2 and high Fe Zircaloy. This seems to be consistent with previous

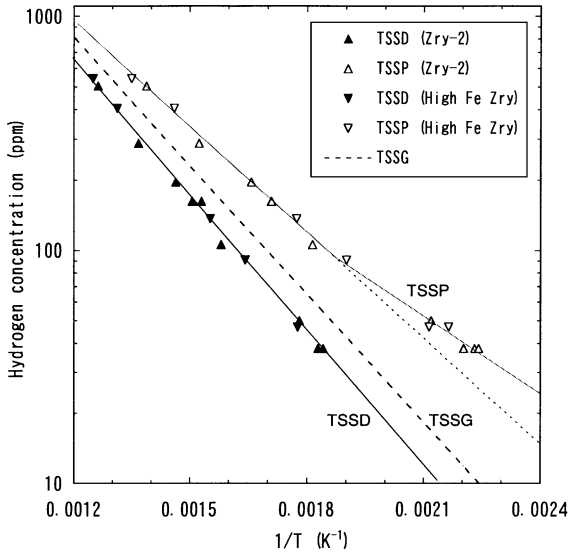

Fig. 3. Solvi of TSSD and TSSP for Zircaloy-2 and high Fe Zircaloy versus reciprocal temperature obtained using DSC.

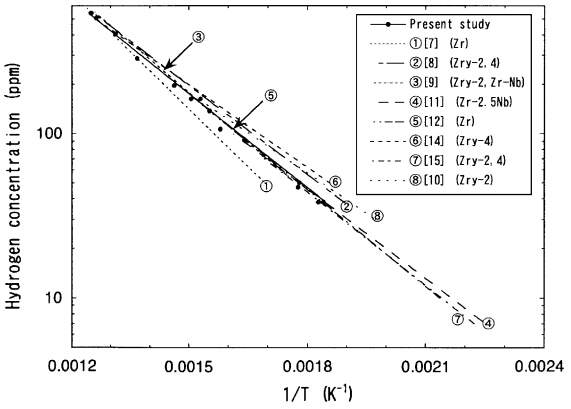

Fig. 4. Comparison of TSSD data obtained by different experimental techniques.

results. Regarding the influence of alloying on TSS, some papers reported almost no alloy effect on TSSD and TSSP. For example, no significant difference was detected in TSSD between Zircaloy-2 and -4 [8], and between Zircaloy-2 and Zr–2.5%Nb [9], and also no difference appeared in TSSP between Zircaloy-2 and -4 [15]. Nevertheless, there is no clear conclusion whether there exists some difference in solubility between Zr and Zircaloys, because no systematic measurements have been made so far. On the other hand, Slattery [10] derived different TSSD and TSSP solvi for Zircaloy-2, Zircaloy-4 and Zr–2.5%Nb.

Best-fit equations for the present TSSD and TSSP solvi of both Zircaloy-2 and high Fe Zircaloy are given by Eqs. (1)–(3) for hydrogen concentrations of 40–542 ppm.

$$C_{\mathrm{TSSD}}\ (\mathrm{ppm}) = 1.28 \times 10^5 \exp(-36\,540/RT), \tag{1}$$

$$C_{\mathrm{TSSP}}\ (\mathrm{ppm}) = 5.26 \times 10^4 \exp(-28\,068/RT) > 533\ \mathrm{K}, \tag{2}$$

$$C_{\mathrm{TSSP}}\ (\mathrm{ppm}) = 1.07 \times 10^4 \exp(-21\,026/RT) \leqslant 533\ \mathrm{K}. \tag{3}$$

Here R is the gas constant (8.314 J/K/mol) and T, the temperature in K. There are two different activation energies for TSSP, separating into high and low temperature ranges at 533 K (260 °C), and there exists a significant hysteresis between TSSD and TSSP solvi.

Fig. 4 compares the present and literature TSSD solvi obtained for Zr, Zircaloy-2, Zircaloy-4 and Zr–2.5%Nb [7–15]. The present activation energy for the hydride dissolution is 36.5 kJ/mol, which is an intermediate value among reported activation energies of 31–45 kJ/mol. In particular, the present energy is in good agreement with the following values: 36.0 kJ/mol by McMinn et al. [15]; 34.5 kJ/mol by Pan et al. [11]; 37.3 kJ/mol by Khatamian and Ling [12]; and 38.9 kJ/mol by Sawatzky and Wilkins [9]. Despite the different experimental techniques used and different ways to define TSSD temperature, when comparing absolute solubilities at a given temperature, the present data are apparently in good accordance with those below 100 ppm by McMinn et al. for Zircaloy-2 and -4 [15] and Pan et al. for Zr–2.5%Nb [11], with those of 10–200 ppm by Khatamian and Ling for Zr [12], and also with those in a wide range of 55–550 ppm by Sawatzky and Wilkins for Zircaloy-2 and Zr–2.5%Nb [9]. These data are somewhat smaller than Kearns's data [8], which have been sometimes referred to as an equilibrium phase boundary for hydrogen in the α-phase.

A comparison of the present and other TSSP data [7,10,11,14,15] is given in Fig. 5. In contrast to the case of TSSD of Fig. 4, a large scatter is seen in TSSP solvi for each investigation. This may result from a non-equilibrium or path-dependent character of TSSP [11,13,15,27–29] and from the difference of measuring technique. The present activation energy of TSSP solvi is best represented as 28.1 kJ/mol in the high temperature range and 21.0 kJ/mol in the low temperature; other investigators have reported values of 21–34 kJ/mol. Assuming one activation energy for the present TSSP in spite of a poorer regression, it would be about 25.4 kJ/mol. The two different activation energies of the present TSSP solvus, separating into high and low temperature ranges at 260 °C, may result from the precipitations of different phases of δ-hydride for the high temperature range, and δ-plus γ-hydride or γ-hydride alone for the low temperature range. There is experimental evidence that, in Zr–2.5wt%Nb, γ-hydride converts to δ-hydride in the temperature range of 180–200 °C [21]. This temperature

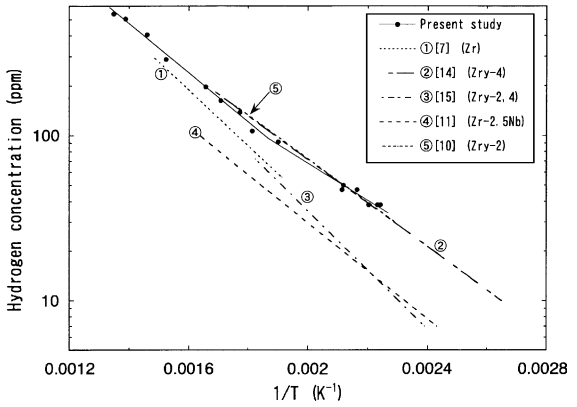

Fig. 5. Comparison of TSSP data obtained by different experimental techniques.

range appears to be consistent with the temperature of 200 °C from the small DSC peak (see Fig. 1) during heatup, which was presumed to correspond to the phase transformation from γ- to δ-hydride. Moreover, the phase transition temperature of 255 °C has been reported for unalloyed Zr from DTA measurements [22].

Comparing absolute solubilities at a given temperature in Fig. 5, we see the present data are consistent with those below 150 ppm by Slattery for Zircaloy-2 [10], and those in a range of 50–500 ppm by Kammenzind et al. for Zircaloy-4 [14]. The literature activation energies were 25.2 kJ/mol by the former, and 25.3 kJ/mol by the latter, which are about 3 kJ/mol larger than the present value of the high temperature range.

3.3. Hysteresis of hydrogen solubility

The large hysteresis seen between the solvi of TSSD and TSSP, has been experimentally and theoretically accepted by many investigators. Basically, it arises from a volumetric misfit strain (approximately 11–17%) between Zr matrix and the less dense hydride phases [19,20,23,24]. Therefore, the TSSP determined on cooldown could be governed by hydride nucleation and the elastic accommodation energy arising from the hydride-matrix misfit. On the other hand, TSSD determined on heatup could be dominated by plastic accommodation effects. In fact, once hydrides precipitate in the Zr matrix, many dislocations surround the hydrides, accompanying plastic deformation [25,26].

Puls [27–29] has advanced a theory for this hysteresis effect, in which the solubility determined on hydride nucleation on cooldown, C_{TSSP}, can be written in terms of the hypothetical or non-constrained equilibrium solubility, $C_{\mathrm{TSS}}(= C_0 \exp(-Q/RT)$; Q: heat of solution of δ-hydride in hydrogen saturated α-Zr(H)), as follows:

$$C_{\mathrm{TSSP}} = C_{\mathrm{TSS}} \exp(w_{\mathrm{el}}/RT), \tag{4}$$

where w_{el} is the total elastic strain energy of matrix and hydride precipitate per mole H. The constrained solvus C_{TSSP} gives the amount of hydrogen that can be maintained in solution up to the first precipitation of hydrides.

The terminal solubility determined on hydride dissolution on heatup, C_{TSSD}, is governed by a balance between the molar plastic accommodation energy w_{p} and the remaining elastic accommodation energy $w_{\mathrm{el,p}}$ in elastic–plastic deformation such that

$$C_{\mathrm{TSSD}} = C_{\mathrm{TSS}} \exp((w_{\mathrm{el,p}} - w_{\mathrm{p}})/RT). \tag{5}$$

The dissolution solvus C_{TSSD} is the solubility boundary in the presence of hydrides that have reached this state as a result of a dissolution process. This would be the case when the temperature of the specimen is approached from below.

In addition to the above two solvi, there is the growth solvus of hydrides, C_{TSSG}, which represents the solubility boundary in the presence of precipitated hydrides that have reached this state as a result of a growth process. This would be the case after nucleation has taken place and with the temperature of the sample approached from above. Then, C_{TSSG} can be expressed by

$$C_{\mathrm{TSSG}} = C_{\mathrm{TSS}} \exp((w_{\mathrm{el,p}} + w_{\mathrm{p}})/RT). \tag{6}$$

In this equation, in comparison to the expression of C_{TSSP}, the total elastic strain energy w_{el} is replaced by its corresponding elastic-plastic value. Based on the assessments of each energy by Puls [28,29], the total elastic strain energy w_{el} is much larger than the total elastic–plastic strain energy $w_{\mathrm{el,p}} + w_{\mathrm{p}}$, and the value of $w_{\mathrm{el,p}} - w_{\mathrm{p}}$ is small and negative. To a first approximation, $C_{\mathrm{TSSD}} \cong C_{\mathrm{TSS}}$. This was the basis for assuming that a heatup solvus of TSSD approximates the stress-free TSS.

A hypothetical curve of C_{TSSG} is drawn in Fig. 3, together with the present data of TSSD and TSSP, assuming that the values of $w_{\mathrm{el,p}} - w_{\mathrm{p}}$ and $w_{\mathrm{el,p}} + w_{\mathrm{p}}$ are roughly −0.2 and 1.3 kJ/mol based on the assessments by Puls [29] and that the pre-exponential constant of C_{TSSG} and C_{TSSD} is the same. In this situation, the energy difference between C_{TSSG} and C_{TSSD} is 1.5 kJ/mol, i.e. $2\ w_{\mathrm{p}} = 1.5$ kJ/mol. The total elastic strain energy w_{el}, which was estimated from the difference in activation energies of the present TSSD and TSSP solvi, is 8.2 kJ/mol for the high temperature region above 260 °C (533 K). This elastic strain energy is roughly double the value assessed by Puls [29]. As seen in Fig. 3, in the low temperature range below 260 °C, a larger elastic energy of about 15 kJ/mol is obtained. The reason for this behavior is not clear, but may correlate with the precipitation of γ-hydride at these temperatures. It should be noted that the above energy theory excludes actual morphology (size and number density) of hydride precipitates, which must influence the value of each energy.

As an index for the magnitude of the thermal hysteresis of hydrogen solubility, $\Delta T/T_{\mathrm{TSSP}}$ may be derived,

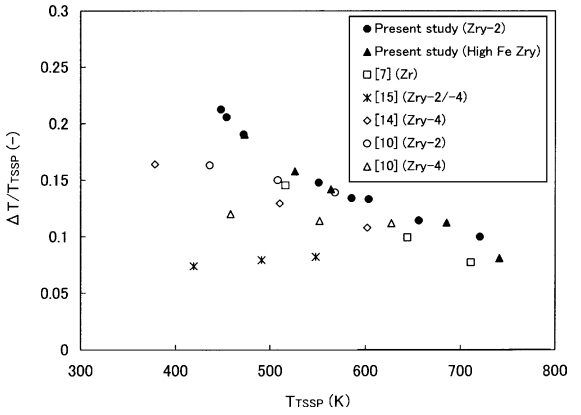

Fig. 6. Thermal hysteresis as a function of TSSP precipitation temperature.

where $\Delta T = T_{TSSD} - T_{TSSP}$, and T_{TSSD} and T_{TSSP} are the dissolution and precipitation temperatures of hydrides at a given hydrogen concentration. Thus the value of $\Delta T/T_{TSSP}$ is closely related to the magnitude of elastic strain energy for the hydride precipitation, and it is naturally temperature dependent. In Fig. 6, the values of $\Delta T/T_{TSSP}$ are plotted against TSSP temperature, together with other literature data [7,10,14,15]. The present data are in good accordance with the results by Erickson et al. [7] and Slattery [10] at higher precipitation temperatures above 220 °C (493 K).

3.4. Average hydride precipitation rate

When Zr hydride precipitates for the first time from a completely dissolved state of hydrogen, super-saturated amounts of hydrogen tend to precipitate during a shorter time, presenting a sharp DSC peak as seen in Fig. 2. Thus the peak width would reflect the average time response of a mixed process of hydride nucleation and growth. Strictly speaking, since hydrogen content in solution and temperature continuously vary during the short peak width, the derived precipitation rates represent solely apparent (mixture of hydride nucleation and growth) and average values. Moreover, this idea to utilize the DSC peak during cooldown is only valid for cases in which the duration of the precipitation reaction is longer than the time response (about 10–20 s) of the present DSC instrument. In this evaluation, the precipitation duration was derived from extrapolated starting and completion temperatures of the DSC peak, and from the cooling rate used, 10 °C/min. Then an average precipitation rate, as a first approximation, was calculated from precipitation duration and super-saturated amounts of hydrogen, which may be regarded as the difference in hydrogen solubility between TSSP and TSSG at the precipitation temperature.

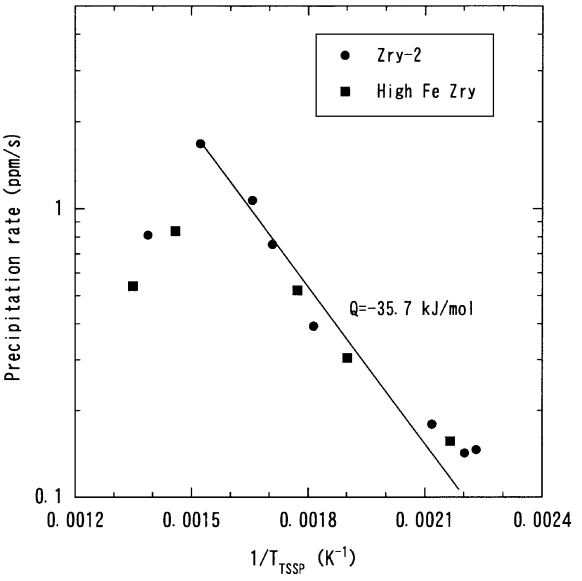

Fig. 7. Average precipitation rate of hydride as a function of temperature derived from the DSC peak on cooldown.

Fig. 7 plots the average precipitation rate of hydride for Zircaloy-2 and high Fe Zircaloy, evaluated from the DSC peak width, against the inverse of absolute temperature. Except for high temperature data above 380 °C (653 K), an Arrhenius-type plot seems to be roughly valid, representing an activation energy of 35.7 kJ/mol, which is expressed by

$$H_P \text{ (ppm/s)} = 1.18 \times 10^3 \exp(-35716/RT). \quad (7)$$

The present activation energy is approximately equivalent to the activation energies (26–43 kJ/mol) of hydrogen or tritium diffusion in Zr and Zircaloys [14,30–34], which may suggest that the overall hydride precipitation is rate-controlled by the diffusion of hydrogen. An abrupt drop and not-thermally activated behavior of the precipitation rate above 380 °C probably indicates a change of the kinetic mechanism, because the peak widened significantly with higher temperatures above 380 °C, in contrast to the opposite tendency in the lower temperature range. Two factors may influence the kinetics: (1) a trapping effect for hydrogen diffusion by defect clusters such as dislocations and (2) a remarkable difference in morphology (size and number density) of hydride nuclei formed in low and high temperature regions. For a clarification of the mechanism, more appropriate experimental work is needed. Kammenzind et al. [14] have reported overall hydride precipitation rates of 1–4 ppm/s, which were derived from diffusion profiles of hydrogen in Zircaloy-4 corroded in concentrated lithiated water at 288–360 °C. Their rates are about two times larger than the present data of 0.5–1.7 ppm/s at the corresponding temperatures.

4. Conclusions

The terminal solid solubility during the dissolution of hydrides (TSSD) at heatup and during the precipitation of hydrides (TSSP) at cooldown were measured for hydrogenated Zircaloy-2 and high Fe Zircaloy in the temperature range of 50–600 °C, using DSC. The hydrogen concentrations in the two kinds of alloys ranged from 40 to 542 ppm. There was no difference in either TSSD or TSSP solvi between Zircaloy-2 and high Fe Zircaloy, and best-fit equations were derived for the two solvi. In the present TSSP solvus, two different activation energies, separating into high and low temperature ranges at 260 °C (533 K) were obtained. The thermal hysteresis between TSSD and TSSP solvi became larger with lower temperatures:

$$C_{\mathrm{TSSD}}\ (\mathrm{ppm}) = 1.28 \times 10^5 \exp(-36\,540\ (\mathrm{J/mol})/RT),$$

$$C_{\mathrm{TSSP}}\ (\mathrm{ppm}) = 5.26 \times 10^4 \exp(-28\,068\ (\mathrm{J/mol})/RT) > 533\ \mathrm{K},$$

$$C_{\mathrm{TSSP}}\ (\mathrm{ppm}) = 1.07 \times 10^4 \exp(-21\,026\ (\mathrm{J/mol})/RT) \leqslant 533\ \mathrm{K}.$$

Based on the widths of the DSC peak obtained during cooldown, the average precipitation (nucleation plus growth) rates H_{P} of zirconium hydride from supersaturated state were evaluated as

$$H_{\mathrm{P}}\ (\mathrm{ppm/s}) = 1.18 \times 10^3 \times \exp(-35\,716\ (\mathrm{J/mol})/RT) \leqslant 653\ \mathrm{K}.$$

The activation energy of the precipitation rate was approximately consistent with reported values of hydrogen diffusion coefficients of Zr and Zircaloys, which may suggest a hydrogen diffusion mechanism. At higher temperatures above 380 °C (653 K), a different mechanism would have to be considered.

References

[1] D.O. Northwood, U. Kasasih, Int. Met. Rev. 28 (1983) 92.
[2] B. Cox, J. Nucl. Mater. 170 (1990) 1.
[3] K. Edsinger, J.H. Davies, R.B. Adamson, Zirconium in the Nuclear Industry: Twelfth Int. Symp., ASTM STP1354, 2000, p. 316.
[4] K. Edsinger, Proceedings of the International Topical Meeting on LWR Fuel Performance, Park City, 10–13 April 2000, p. 523.
[5] Summary Report on The Verification Test on BWR High Burnup Fuel, Nuclear Power Engineering Corporation (NUPEC), March 2002.
[6] S. Shimada et al., J. Nucl. Mater, in press.
[7] W.H. Erikson, D. Hardie, J. Nucl. Mater. 13 (1964) 254.
[8] J.J. Kearns, J. Nucl. Mater. 22 (1967) 292.
[9] A. Sawatzky, B.J.S. Wilkins, J. Nucl. Mater. 22 (1967) 304.
[10] G.F. Slattery, J. Ins. Metals 95 (1967) 43.
[11] Z.L. Pan, I.G. Ritchie, M.P. Puls, J. Nucl. Mater. 228 (1996) 227.
[12] D. Khatamian, V.C. Ling, J. Alloy Comp. 253 (1997) 162.
[13] D. Khatamian, Z.L. Pan, M.P. Puls, C.D. Cann, J. Alloy Comp. 231 (1995) 488.
[14] B. Kammenzind, D.G. Franklin, H.R. Peters, W.J. Duffin, Zirconium in the Nuclear Industry: Eleventh Int. Symp., ASTM STP1295, 1997, p. 338.
[15] A. McMinn, E.C. Darby, J.S. Schofield, Zirconium in the Nuclear Industry: Twelfth Int. Symp., ASTM STP1354, 2000, p. 173.
[16] S. Ishimoto, T. Kubo, R.B. Adamson, Y. Etoh, K. Ito, Y. Suzawa, Proceedings of the International Topical Meeting on LWR Fuel Performance, Park City, 10–13 April 2000, p. 499.
[17] M. Amaya, K. Une, K. Minato, J. Nucl. Mater. 294 (2001) 1.
[18] K. Une, S. Ishimoto, J. Nucl. Mater., in press.
[19] F. Zuzek, J.P. Abriata, Bull. Alloy Phase Diagrams 11 (1990) 385.
[20] A. Aladjem, in: F.A. Lewis, A. Aladjem (Eds.), Hydrogen Metal System I, Balaban, 1996 (Chapter 7).
[21] J.H. Root, R.W.L. Fong, J. Nucl. Mater. 232 (1996) 75.
[22] S.M. Mishra, K.S. Sivaramakrishnan, M.K. Asundi, J. Nucl. Mater. 45 (1972) 235.
[23] H. Numakura, T. Ito, M. Koiwa, J. Less-Common Met. 141 (1988) 285.
[24] G.J.C. Carpenter, J. Nucl. Mater. 48 (1973) 264.
[25] J.E. Bailey, Acta Metall. 11 (1963) 267.
[26] G.J.C. Carpenter, J.F. Watters, J. Nucl. Mater. 73 (1978) 190.
[27] M.P. Puls, Acta Metall. 32 (1984) 1259.
[28] M.P. Puls, Metall. Trans. A 21 (1986) 2905.
[29] M.P. Puls, J. Nucl. Mater. 165 (1989) 128.
[30] M.W. Mallet, W.M. Albrecht, J. Electrochem. Soc. 104 (1957) 142.
[31] A. Sawatzky, J. Nucl. Mater. 2 (1960) 62.
[32] J.J. Kearns, J. Nucl. Mater. 43 (1972) 330.
[33] F.M. Muzzolai, J. Ryll-Nardzewski, J. Less-Common Met. 49 (1976) 323.
[34] G.U. Greger, H. Munzel, W. Kung, J. Nucl. Mater. 88 (1980) 15.